Coherent extreme ultraviolet free-electron laser with echo-enabled harmonic generation

Chao Feng, Haixiao Deng, Meng Zhang, Xingtao Wang, Si Chen, Tao Liu, Kaishang Zhou, Duan Gu, Zhen Wang, Zenggong Jiang, Xuan Li, Baoliang Wang, Wenyan Zhang, Taihe Lan, Lie Feng, Bo Liu, Qiang Gu, Yongbin Leng, Lixin Yin, Dong Wang, and Zhentang Zhao*

Shanghai Advanced Research Institute, Chinese Academy of Sciences, Shanghai 201210, China

Guanglei Wang

State Key Laboratory of Molecular Reaction Dynamics, Dalian Institute of Chemical Physics, Chinese Academy of Sciences, Dalian 116023, People's Republic of China

Dao Xiang

Key Laboratory for Laser Plasmas (Ministry of Education), School of Physics and Astronomy, Shanghai Jiao Tong University, Shanghai 200240, China

(Received 27 February 2019; published 17 May 2019)

The echo-enabled harmonic generation (EEHG) scheme holds promising prospects for efficiently generating intense coherent radiation at very high harmonics of a conventional ultraviolet seed laser. We report the lasing of the EEHG free-electron laser (FEL) at an extreme ultraviolet (EUV) wavelength with a seeded FEL facility, the Shanghai soft x-ray FEL. For the first time, we have benchmarked the basic theory of EEHG by measuring the bunching factor distributions over one octave down to the EUV region. Our results demonstrated the key advantages of the EEHG FEL, i.e., generation of very high harmonics with a small laser-induced energy spread and insensitivity to beam imperfections, and marks a great step towards fully coherent x rays with the EEHG scheme.

DOI: 10.1103/PhysRevAccelBeams.22.050703

I. INTRODUCTION

Free-electron lasers (FELs) that are able to provide tunable high-power coherent radiation have a wide array of applications in biology, chemistry, physics, and material science [1]. Several x-ray FEL facilities have been successfully operated around the world [2–9], which marks the beginning of a new era of x-ray sciences. In the x-ray wavelength range, most of the FEL facilities are operated with the self-amplified spontaneous emission (SASE) principle [10,11]. While the SASE scheme allows FEL lasing at a subangstrom wavelength [4], its output has rather limited temporal coherence, as the initial radiation starts from electron beam shot noise. There are many applications such as resonant scattering and spectroscopic techniques that require, or could benefit from, improved temporal coherence.

Several techniques have been developed for seeding short-wavelength FELs with external lasers at ultraviolet (UV) wavelengths to generate stable and fully coherent radiation [12–28]. These techniques all rely on producing bunching at the harmonic frequency of the seed laser. In the high-gain harmonic generation (HGHG) [12,13] technique, sinusoidal energy modulation in beam longitudinal phase space is first produced through a laser-electron interaction in a short undulator (modulator). After passing through a small chicane, the energy modulation is converted into density modulation that has a frequency component at the harmonic frequency of the seed laser. Finally, the density-modulated beam is sent through a long undulator (radiator) where the bunching produces a coherent signal that is further amplified with the FEL process to generate radiation with enhanced temporal coherence. Because the bunching at the ath harmonic requires the energy modulation to be approximately a times larger than the beam slice energy spread, single-stage HGHG FELs have limited frequency up-conversion efficiency [13]. As a result, multiple stages of HGHG are typically required to reach x-ray wavelengths starting from a UV seed laser [17–19], and the stability, in general, has an increased sensitivity to beam fluctuations [19]. Furthermore, the central wavelength and bandwidth of

*zhaozhentang@sinap.ac.cn

Published by the American Physical Society under the terms of the Creative Commons Attribution 4.0 International license. Further distribution of this work must maintain attribution to the author(s) and the published article's title, journal citation, and DOI.

a HGHG FEL are sensitive to beam imperfections, in particular, linear and nonlinear energy chirps [29,30].

These limitations may be overcome with the echo-enabled harmonic generation (EEHG) technique [20,21], which employs two modulator-chicane modules to imprint strong bunching on the electron beam. By using a strong chicane with large momentum compaction to split the phase space that produces energy bands with a small slice energy spread, only a relatively small energy modulation is needed to produce high harmonic bunching. Furthermore, the highly nonlinear phase space manipulation process inherent to the EEHG technique also efficiently damps initial linear and nonlinear correlations in beam longitudinal phase space, leading to an enhanced insensitivity to beam imperfections.

These advantages have stimulated worldwide efforts in exploring the potential of the EEHG technique for producing fully coherent x rays in FELs. Initial proof-of-principle experiments demonstrated bunching up to the 15th harmonic [24–26] and lasing at the 3rd harmonic (∼350 nm) [27] with a seed laser in the far-infrared (FIR) wavelength. Recently, coherent emission with the EEHG technique at the 75th harmonic (∼32 nm) of a 2400 nm seed laser was also reported [28]. While the basic physics behind the EEHG scheme has been demonstrated with a FIR seed laser, benchmarking the EEHG theory with a UV seed laser in a large parameter space has not been achieved. Furthermore, there is concern that the strong chicane used in the EEHG technique may amplify the initial beam instability and lead to unwanted effects that might outweigh its advantages. Therefore, experiments with realistic parameter sets, e.g., UV seed lasers and a compressed electron beam with a high peak current, are highly desired to demonstrate the full feasibility of EEHG for an x-ray FEL facility.

Here we report the first lasing of an EUV FEL at 24 nm and coherent emission down to 8.9 nm with the EEHG technique at the Shanghai soft x-ray FEL facility (SXFEL) [31]. The lasing wavelength is one order of magnitude shorter than that achieved in a previous experiment and comparable also in terms of harmonics to the ongoing experiments at Fermi. For the first time, with this experiment the bunching factor distributions of EEHG have been measured over one octave and are found to be in excellent agreement with the EEHG theory. Comparing with HGHG, our experimental results clearly show the higher-frequency up-conversion efficiency and less sensitivity to beam imperfections of EEHG and pave the way towards coherent, intense, and stable x rays.

II. EXPERIMENTAL RESULTS

A. Experimental setup

The accelerator of the SXFEL consists of a photo-injector, a linac with S-band and C-band accelerator structures, and a magnetic bunch compressor. The electron beam energy E at the end of the linac can be tuned from 500 to 670 MeV with a transverse emittance of about 2 μm rad and the peak current over 500 A. The undulator system of the SXFEL aims to produce EUV and soft x-ray radiation from a 266 nm conventional seed laser through a two-stage cascaded HGHG scheme, as shown in Fig. 1. Each stage consists of a modulator, a dispersion section, and a radiator. These two stages are connected by a fresh bunch (FB) chicane.

Two options to implement the EEHG scheme based on the existing undulator system have been studied with numerical simulations before the experiment [32]. Both options use the two modulator-chicane modules in the two stages to produce the required energy modulation and density modulation and then send the bunched electron beam into the R2 with six undulator segments for FEL amplification. For the first option where DS1 is used to split the phase space, the gap of the R1 in the first stage is accordingly completely open and the FB chicane is tuned off. However, for this setup, simulation results [32] indicate that the intrabeam scattering, longitudinal space charge, and second-order transport effects in the long drift section from DS1 to M2 will significantly degrade the fine structures of EEHG. In the second option, DS1 and R1 were turned off, and the strength of the FB chicane is increased to function as the strong chicane to split the beam phase space. An analysis shows that for this option, because no fine structures are generated before the FB chicane, the energy modulation from M1 can be well preserved in the long drift from M1 to the FB chicane. The EEHG experiment is based on the second option, as shown in Fig. 1. The main parameters used during the EEHG experiment are given in Table I, where λ_u is the period length, N_p is the period number of one segment undulator, and R_{56} is the

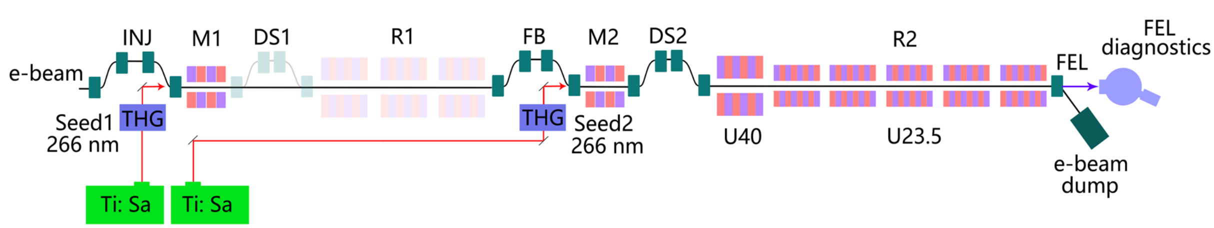

FIG. 1. Layout of the EEHG experiment at the SXFEL. INJ, injection chicane; M, modulator; FB, fresh-bunch chicane; DS, dispersion section; R, radiator.

TABLE I. Main parameters of the EEHG experiment.

Electron beam	
Beam energy	500–670 MeV
Bunch charge	500 pC
Slice energy spread	30–40 keV
Project energy spread	1 MeV
Project emittance	2 mm mrad
Peak current	>500 A
Bunch length (FWHM)	1 ps
Seed laser	
Seed laser wavelength	266 nm
Seed laser pulse length (FWHM)	1 ps
Undulator system	
$N_p \times \lambda_u$ for M1	20×8 cm
$N_p \times \lambda_u$ for M2	36×5.5 cm
$N_p \times \lambda_u$ for R	120×2.35 cm
R_{56} of DS1 (R_{56}^1)	0–10 mm
R_{56} of DS2 (R_{56}^2)	0–2 mm

dispersive strength of the chicane. One of the critical parameters for the parameter setting of EEHG is the slice energy spread, which is measured to be about 30–40 keV (depending on different compression ratios) by the coherent harmonic-generation-based method [33].

Two UV laser systems are adopted for the two seed lasers (seed 1 and seed 2) of EEHG to achieve a higher seed power. The pulse lengths of these two seed lasers are tuned to 1 ps to fully cover the electron bunch, which will be helpful to illustrate the sensitivity of the FEL output to beam linear and nonlinear energy chirps. Laser-electron beam interactions were achieved when the electron beam and laser beam overlapped spatially and temporally in modulators. The FEL properties can be detected by the FEL diagnostics station located by the end of the radiator, which consists of a fluorescence screen for detecting the FEL transverse spot, a photodiode for measuring FEL pulse energy, and a spectrometer that can cover the wavelength range of 5–25 nm.

B. Benchmark the theory of EEHG in EUV region

As mentioned above, the key advantage of EEHG is, by manipulating the longitudinal phase space of the electron beam with a large chicane, very small-scale coherent microbunchings can be generated from separated energy bands with a relative small energy modulation. As a result, the up-conversion efficiency will be enhanced only for the target high harmonics, which is close to the ratio R_{56}^1/R_{56}^2. In contrast, the bunching factor of HGHG shows exponential behavior, and bunching at many harmonics will all be produced. The harmonic up-conversion efficiency can be quantified by the bunching factor, which can be calculated for HGHG and EEHG by [12,21]

$$b_a = |J_a(-aAB)e^{-(1/2)a^2B^2}|, \tag{1}$$

$$b_{n,m} = |J_n\{-A_1[nB_1 + (Km+n)B_2]J_m \times [-(Km+n)A_2B_2]\}e^{-(1/2)[nB_1+(Km+n)B_2]^2}|, \tag{2}$$

where A is the energy modulation amplitude divided by the energy spread σ_E, $B = R_{56}k\sigma_E/E$, k is the wave number of the seed laser, $K = k_2/k_1$, a is the harmonic number for HGHG, and $a = m + n$ for EEHG.

Comparing with HGHG, the optimized condition is more complicated for EEHG, whose bunching factor is determined by the combination of four parameters for a given harmonic number. One novelty of our experiment is measuring and comparing the bunching factor distributions of HGHG and EEHG over one octave in frequency in the EUV region, via direct measurement of the coherent radiation intensities for various harmonics. To allow benchmarking the theory in such a large parameter space, we removed the first undulator segment of R2 (U23.5) and replaced it with an undulator with a longer period (U40) from R1, which can cover the harmonic number range from 6th to 20th (13.3–44 nm) by tuning the magnetic gap from 15 to 30 mm with the electron beam energy of 670 MeV. The intensity of the coherent radiation is proportional to the square of the bunching factor and can be detected by the photodiode at the end of R2.

Figure 2 shows the measurement results for both HGHG and EEHG. In the experiments, seed 2 was first turned on to

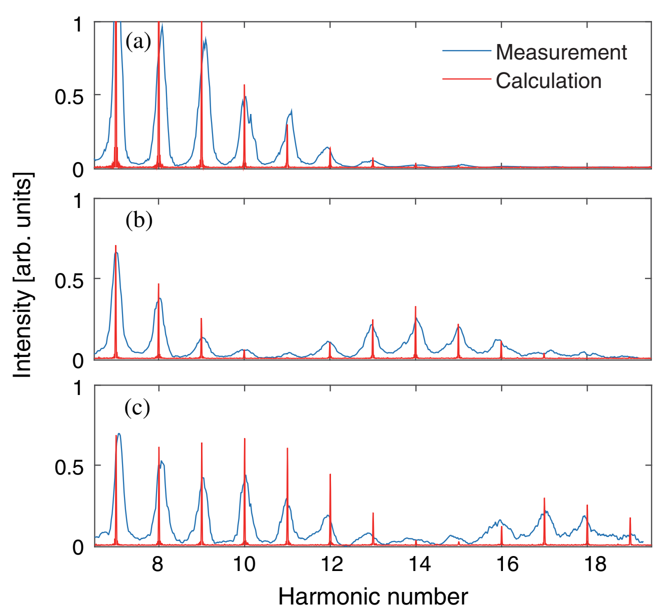

FIG. 2. Comparison of coherent radiation intensities at various harmonic numbers for single-stage HGHG and EEHG. (a) HGHG: $A_1 = 0$, $A_2 = 8.5$, $R_{56}^1 = 1.0$ mm, and $R_{56}^2 = 90\ \mu$m; (b) EEHG: $A_1 = 2.5$, $A_2 = 8.5$, $R_{56}^1 = 1.0$ mm, and $R_{56}^2 = 90\ \mu$m; (c) EEHG: $A_1 = 2.5$, $A_2 = 8.5$, $R_{56}^1 = 1.45$ mm, and $R_{56}^2 = 90\ \mu$m.

interact with the electron beam in M2 and R^1_{56} was set to 1 mm. The laser power was increased to the maximal value to allow the generation of harmonics in HGHG as high as possible. The DS2 were scanned to find the maximal radiation power with the R^2_{56} of around 90 μm, which indicates an energy modulation amplitude of about 300 keV according to Eq. (1). After that, the gap of U40 has been continually tuned from 15 to 30 mm to generate coherent radiation at various harmonics. The power of the coherent radiation is proportional to $K_R^2[JJ]^2 b_a^2$, where K_R^2 is the dimensionless undulator parameter and $[JJ] = J_0[K_R^2/(4+2K_R^2)] - J_1[K_R^2/(4+2K_R^2)]$ is the coupling factor of the planar undulator. By normalizing the radiation power with the $K_R^2[JJ]^2$ and response sensitivity of the photodiode for different wavelengths, we found that the radiation intensity of HGHG decreased exponentially with the harmonic number, as shown in Fig. 2(a), which fits quite well with the calculations based on Eq. (1) with the same parameters. The broadening of each harmonic is mainly caused by the gain bandwidth of the undulator and the large energy chirp in the electron beam. With the full power of the seed laser, the highest harmonic number of HGHG achieved is about 15. Then, we turn on the first seed laser for testing the EEHG setup. The energy modulation amplitude induced by seed 1 is about 100 keV, which is measured by scanning the R^1_{56} and finding the maximal radiation power from M2. The measurement results are shown in Fig. 2(b), where one can find that the intensity of EEHG at low harmonics is lower than HGHG due to the extra energy spread induced by seed 1; however, a cluster of bunching factor appears around the target high harmonic, which can be much higher than that of HGHG. This cluster of bunching factor can be continually shifted to higher harmonics by simply increasing R^1_{56} from 1 to 1.45 mm (the timing of seed 2 has been accordingly delayed), as shown in Fig. 2(c), in agreement with the scaling $a \sim R^1_{56}/R^2_{56}$. The intensity for the optimized high harmonics can be well maintained, which means that the bunching factor of EEHG decreases slowly with the harmonic number. These experiment results coincide with the theoretical predictions and also fit quite well with calculations.

In addition, R^2_{56} was scanned for various values of A_2 to further benchmark the theory. An analysis using Eq. (2) indicates that, in general, there are multiple parameter sets that can lead to considerable bunching. As a result, many islands could be seen in the bunching distribution of EEHG. For instance, with $A_1 = 3.5$ and $R^1_{56} = 2.2$ mm, the theoretical bunching distributions at the 20th harmonic for various A_2 and R^2_{56} are shown in Fig. 3(a). Figure 3(b) shows the measured radiation intensity at the 20th harmonic as a function of R^2_{56} with A_2 set to 6.3. Significant radiation is observed only at the optimized R^2_{56} value of 0.13 mm. The results are in good agreement with the theoretical values [red dashed line in Fig. 3(a)]. In a separate experiment, A_2 was lowered to 5, and the measured radiation intensity for various R^2_{56} is shown in Fig. 3(c), where one can clearly see the "double peak" structure. The results are also found to be in good agreement with the calculations [white dashed line in Fig. 3(a)]. It is worth pointing out that, in Fig. 3(c), the radiation intensity at the second peak ($R^2_{56} = 0.163$ mm) is much more stable than the first one ($R^2_{56} = 0.136$ mm). Theoretical analyses in Fig. 3(a) (white dashed line) show that the second peak is located at the local optimized point, while the first one is at a ramping region which is more sensitive to A_2. With a power fluctuation of about 4% of seed 2, calculation results indicate an output power fluctuation of about 60% (peak to peak) for the first peak, which, again, is in good agreement with the experimental results.

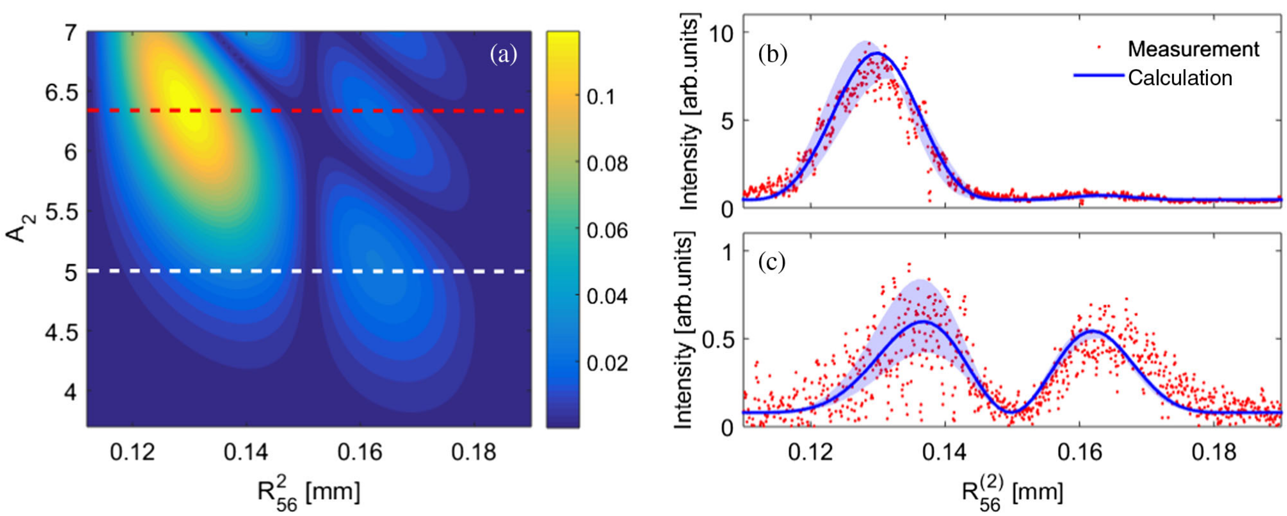

FIG. 3. (a) Theoretical bunching distributions for $A_1 = 3.5$ and $R^1_{56} = 2.2$ mm. Measured intensity of the coherent radiation at the 20th harmonic as a function of R^2_{56} for $A_2 = 6.3$ (b) and $A_2 = 5$ (c). The blue shadow in (b) and (c) represents the calculation results with a power fluctuation of 4% for the second seed laser.

C. COHERENT RADIATION IN THE EUV AND X-RAY REGION FROM EEHG

The coherent signal of EEHG can be further amplified by the following undulator segments of R2 with a period length of 23.5 mm. To facilitate the comparison of HGHG and EEHG spectra in the presence of beam imperfections, we amplified HGHG and EEHG at the 11th harmonic (24.2 nm) of the seed, where both HGHG and EEHG have sufficient bunching factors. With the same energy modulation amplitudes of $A_2 = 8.5$, the total laser-induced energy spread for EEHG with two seed lasers is larger than HGHG, which results in a higher saturation power of HGHG. However, we can reduce the seed laser power and correspondingly increase the two DS strengths of EEHG to reduce the laser-induced energy spread and maintain the bunching factor. In our experiment, the A_2 of EEHG had been reduced by over 2 times by tuning the attenuator, and the R^1_{56} and R^2_{56} had been accordingly increased to about 1.55 and 0.16 mm, respectively. It is worth pointing out here that no coherent signal at the 11th harmonic is observed from HGHG for the reduced energy modulation amplitude of $A_2 = 4$. The measured gain curves of HGHG for $A_2 = 8.5$ and EEHG for $A_1 = 2.5$ and $A_2 = 4$ are shown in Fig. 4(a). HGHG got saturation inside the 4th undulator with a pulse energy of about 190 μJ. EEHG generated a slightly higher saturation pulse energy of about 230 μJ. The gain length for HGHG and EEHG is 1.33 and 1.25 m, respectively, fitting reasonably well with the Genesis [34] simulations with the same parameters. The slightly shorter gain length and higher saturation power of EEHG are mainly due to the reduced beam energy spread.

Figure 4(b) shows the spectra of HGHG and EEHG, where one can see that EEHG has a higher spectral brightness and narrower bandwidth. The relative bandwidth (FWHM) for EEHG is about 6×10^{-4}, while that for HGHG is about 3×10^{-3}. In addition, the central wavelength of the EEHG scheme is at 24.16 nm, while that for the HGHG scheme is at 24.09 nm. The difference in bandwidth and central wavelength is mainly due to correlations in beam phase space. Figure 4(c) shows the electron beam longitudinal phase space measured with an X-band deflector at the linac exit, where considerable linear and nonlinear energy chirps superimposed with high-frequency modulations from microbunching instability can be seen. As predicted by the theory [29,30], the spectra of HGHG and EEHG have different responses for the energy curvature in the electron beam. A linear energy chirp in the electron beam together with the strength of the DS will shift the central frequency of HGHG by $k_h = a/k_2(1 + hR^2_{56})$, where $h = d\delta/dz$ is the energy chirp and δ is the relative beam energy change along the longitudinal direction z. This effect will broaden the bandwidth if the chirp also varies in z. In contrast, EEHG can be made nearly immune to the energy chirp under the optimized strengths of the two dispersions. As shown in Fig. 4(c), the beam core [from 0.5 to 1.2 ps in

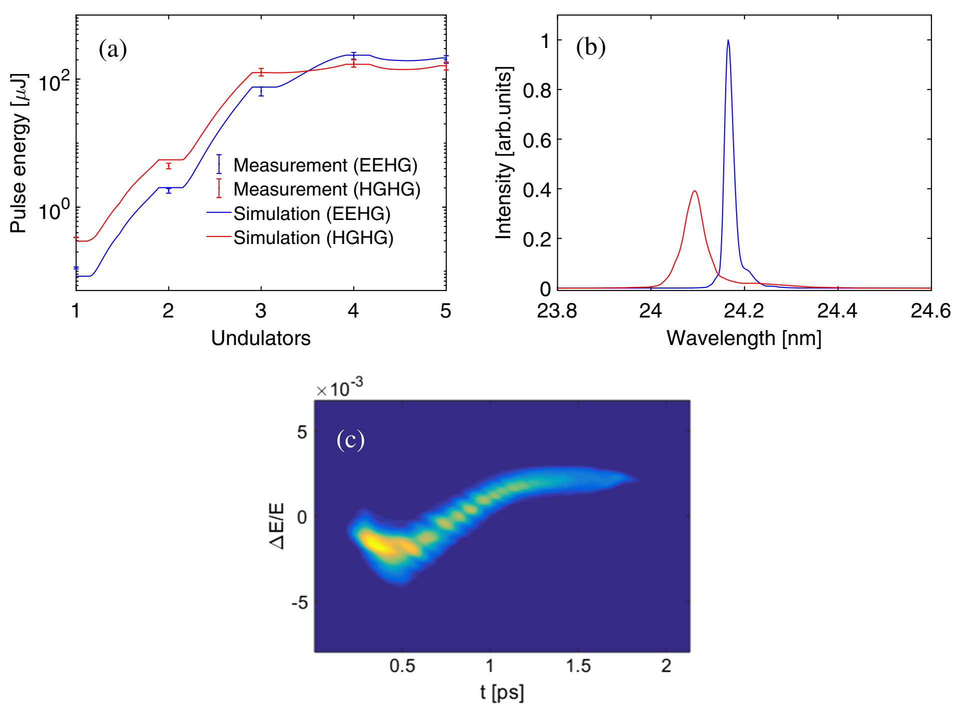

FIG. 4. Comparison of FEL gain curves (a) and spectra (b) for HGHG and EEHG at the 11th harmonic of the seed lasers (accumulated by 50 consecutive shots). (c) Measurement results of the longitudinal phase space of the electron beam by the X-band deflecting cavity at the end of the linac (bunch head to the left).

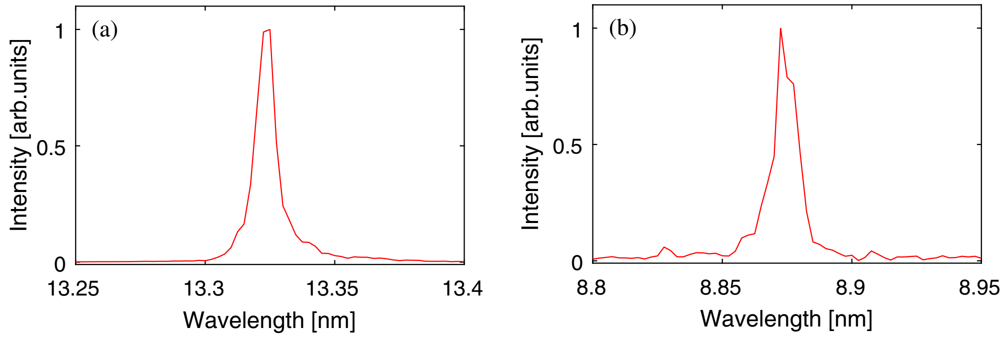

FIG. 5. Output spectra of EEHG at 20th and 30th harmonics of the seed laser (accumulated with integration over 50 shots).

Fig. 4(c)] has approximately a linear energy chirp of about 16 m^{-1}, which is responsible for the central wavelength shift of about 0.07 nm for HGHG. The electron beam also contains a large residual quadratic energy chirp induced by the wakefield of the C-band linac, which results in a bandwidth broadening of about 0.06 nm for HGHG. These measurement results fit quite well with the theoretical calculations. In contrast, the wavelength shift and spectrum broadening are negligible for EEHG, which leads to a 5 times narrower bandwidth compared to HGHG. We can also find in Fig. 4(b) that both the spectra have significant pedestal-like sidebands at the bottom, which is likely caused by the strong microbunching instability (MBI) in the electron beam [Fig. 4(c)] due to the lacking of laser heater system at the present SXFEL.

Limited by the beam quality (affected by the MBI), lasing at higher harmonics was not achieved. Nevertheless, by changing the ratio of R^1_{56} and R^2_{56}, the bunching can still be optimized at higher harmonics, and a coherent radiation signal at the level of a few microjoules has also been measured for the 20th (13.3 nm) and 30th (8.8 nm) harmonics of the seed laser with EEHG, and the measured spectra are shown in Fig. 5. The relative bandwidth of the spectra at the 20th and 30th harmonics are about 6.7×10^{-4} and 1.0×10^{-3}, respectively, which are limited by the resolution of the spectrometer (0.005 nm). It should be pointed out that in this experiment the 30th harmonic was produced with $A_2 = 5$, again demonstrating the key advantage of EEHG in producing high harmonics with a relatively small energy modulation.

III. CONCLUSIONS

We have reported the first lasing of an EUV FEL at 24 nm and the observation of coherent emission down to 8.9 nm with the EEHG technique at the SXFEL. The bunching factor distributions of EEHG have been benchmarked with the theory in a large parameter space, allowing the confirmation of predictive models and scaling laws. We have compared the performances of single-stage HGHG and EEHG at the EUV wavelength and demonstrated high-frequency up-conversion efficiency of EEHG and the insensitivity of EEHG to beam imperfections, marking a great step toward EEHG at soft x-ray wavelengths. Analyses within the framework of idealized models also indicate the possibility of generating coherent radiation pulse at subnanometer wavelengths by combining the EEHG scheme with the fresh bunch techniques [35,36]. This kind of laserlike FEL may enable many new areas of sciences and improve the experimental capabilities when compared to the existing EUV and x-ray light sources. The SXFEL will be upgraded to a user facility in the near future with a laser heater system, and lasing of EEHG at higher harmonics would be explored then.

ACKNOWLEDGMENTS

The authors thank Enrico Allaria, Primož Rebernik Ribic, and Erik Hemsing for helpful discussions and useful comments. This work was supported by the National Development and Reform Commission ([2013]2347), the National Natural Science Foundation of China (Grants No. 11605277 and No. 11475250), and the National Key Research and Development Program of China (Grants No. 2016YFA0401901 and No. 2015CB859700).

[1] C. Bostedt, S. Boutet, D. M. Fritz, Z. Huang, H. J. Lee, H. T. Lemke, A. Robert, W. F. Schlotter, J. J. Turner, and G. J. Williams, Linac coherent light source: The first five years, Rev. Mod. Phys. **88**, 015007 (2016).

[2] W. Ackermann et al., Operation of a free-electron laser from the extreme ultraviolet to the water window, Nat. Photonics **1**, 336 (2007).

[3] P. Emma et al., First lasing and operation of an ångstrom-wavelength free-electron laser, Nat. Photonics **4**, 641 (2010).

[4] T. Ishikawa et al., A compact x-ray free-electron laser emitting in the sub-angstrom region, Nat. Photonics **6**, 540 (2012).

[5] E. Allaria et al., The FERMI free-electron lasers, J. Synchrotron Radiat. **22**, 485 (2015).

[6] H. Kang et al., Hard x-ray free-electron laser with femtosecond-scale timing jitter, Nat. Photonics **11**, 708 (2017).

[7] M. Scholz, FEL performance achieved at European XFEL, in *Proceedings of the 9th International Particle Accelerator Conference, Vancouver, BC, Canada, 2018* (JACoW, Geneva, Switzerland, 2018), p. 29.

[8] C. Milne *et al.*, SwissFEL: The Swiss X-ray free electron laser, Appl. Sci. **7**, 720 (2017).

[9] C. Pellegrini, A. Marinelli, and S. Reiche, The physics of x-ray free-electron lasers, Rev. Mod. Phys. **88**, 015006 (2016).

[10] A. Kondratenko and E. Saldin, Generating of coherent radiation by a relativistic electron beam in an undulator, Part. Accel. **10**, 207 (1980).

[11] R. Bonifacio, C. Pellegrini, and L. M. Narducci, Collective instabilities and high-gain regime in a free electron laser, Opt. Commun. **50**, 373 (1984).

[12] L. H. Yu, Generation of intense UV radiation by subharmonically seeded single-pass free-electron lasers, Phys. Rev. A **44**, 5178 (1991).

[13] E. Allaria *et al.*, Highly coherent and stable pulses from the FERMI seeded free-electron laser in the extreme ultraviolet, Nat. Photonics **6**, 699 (2012).

[14] E. Allaria and G. De Ninno, Soft-X-Ray Coherent Radiation Using a Single-Cascade Free-Electron Laser, Phys. Rev. Lett. **99**, 014801 (2007).

[15] M. Labat *et al.*, High-Gain Harmonic-Generation Free-Electron Laser Seeded by Harmonics Generated in Gas, Phys. Rev. Lett. **107**, 224801 (2011).

[16] L. Giannessi *et al.*, High-Order-Harmonic Generation and Superradiance in a Seeded Free-Electron Laser, Phys. Rev. Lett. **108**, 164801 (2012).

[17] L. H. Yu and I. Ben-Zvi, High-gain harmonic generation of soft x-rays with the "fresh bunch" technique, Nucl. Instrum. Methods Phys. Res., Sect. A **393**, 96 (1997).

[18] B. Liu *et al.*, Demonstration of a widely-tunable and fully-coherent high-gain harmonic-generation free-electron laser, Phys. Rev. ST Accel. Beams **16**, 020704 (2013).

[19] E. Allaria *et al.*, Two-stage seeded soft-x-ray free-electron laser, Nat. Photonics **7**, 913 (2013).

[20] G. Stupakov, Using the Beam-Echo Effect for Generation of Short-Wavelength Radiation, Phys. Rev. Lett. **102**, 074801 (2009).

[21] D. Xiang and G. Stupakov, Echo-enabled harmonic generation free electron laser, Phys. Rev. ST Accel. Beams **12**, 030702 (2009).

[22] H. Deng and C. Feng, Using Off-Resonance Laser Modulation for Beam-Energy-Spread Cooling in Generation of Short-Wavelength Radiation, Phys. Rev. Lett. **111**, 084801 (2013).

[23] C. Feng, H. Deng, D. Wang, and Z. T. Zhao, Phase-merging enhanced harmonic generation free-electron laser, New J. Phys. **16**, 043021 (2014).

[24] D. Xiang *et al.*, Demonstration of the Echo-Enabled Harmonic Generation Technique for Short-Wavelength Seeded Free Electron Lasers, Phys. Rev. Lett. **105**, 114801 (2010).

[25] D. Xiang *et al.*, Evidence of High Harmonics from Echo-Enabled Harmonic Generation for Seeding X-Ray Free Electron Lasers, Phys. Rev. Lett. **108**, 024802 (2012).

[26] E. Hemsing, M. Dunning, C. Hast, T. Raubenheimer, S. Weathersby, and D. Xiang, Highly coherent vacuum ultraviolet radiation at the 15th harmonic with echo-enabled harmonic generation technique, Phys. Rev. ST Accel. Beams **17**, 070702 (2014).

[27] Z. T. Zhao *et al.*, First lasing of an echo-enabled harmonic generation free-electron laser, Nat. Photonics **6**, 360 (2012).

[28] E. Hemsing, M. Dunning, B. Garcia, C. Hast, T. Raubenheimer, G. Stupakov, and D. Xiang, Echo-enabled harmonics up to the 75th order from precisely tailored electron beams, Nat. Photonics **10**, 512 (2016).

[29] C. Feng, D. Wang, and Z. T. Zhao, Study of the energy chirp effects on seeded FEL schemes at SDUV-FEL, in *Proceedings of the 3rd International Particle Accelerator Conference, New Orleans, LA, 2012* (IEEE, Piscataway, NJ, 2012), p. 1724.

[30] G. Penn, Stable, coherent free-electron laser pulses using echo-enabled harmonic generation, Phys. Rev. ST Accel. Beams **17**, 110707 (2014).

[31] Z. T. Zhao *et al.*, SXFEL: A soft x-ray free electron laser in China, Synchrotron Radiat. News **30**, 29 (2017).

[32] C. Feng, D. Huang, H. X. Deng, J. H. Chen, D. Xiang, B. Liu, D. Wang, and Z. T. Zhao, A single stage EEHG at SXFEL for narrow-bandwidth soft x-ray generation, Sci. Bull. **61**, 1202 (2016).

[33] C. Feng, T. Zhang, J. H. Chen, H. X. Deng, M. Zhang, X. T. Wang, B. Liu, T. H. Lan, D. Wang, and Z. T. Zhao, Measurement of the average local energy spread of electron beam via coherent harmonic generation, Phys. Rev. ST Accel. Beams **14**, 090701 (2011).

[34] S. Reiche, GENESIS 1.3: A fully 3D time-dependent FEL simulation code, Nucl. Instrum. Methods Phys. Res., Sect. A **429**, 243 (1999).

[35] C. Feng and Z. T. Zhao, Hard x-ray free-electron laser based on echo-enabled staged harmonic generation scheme Chin. Sci. Bull. **55**, 221 (2010).

[36] Z. T. Zhao, C. Feng, J. H. Chen, and Z. Wang, Two-beam based two-stage EEHG-FEL for coherent hard x-ray generation, Sci. Bull. **61**, 720 (2016).